Research Article Adv. Mater. Lett. 2015, **6**(7), 592-599 Advanced Materials *Letters*

www.amlett.com, www.vbripress.com/aml, DOI: 10.5185/amlett.2015.5876 Published online by the VBRI Press in 2015

Mechanisms of composite-hydroxide-mediated approach for the synthesis of functional ZnO nanostructures and morphological dependent optical emissions

Taj Muhammad Khan[1,2]*, M. Zakria[1], Rana I. Shakoor[1,3], M. Raffi[1], Mushtaq Ahmad[1]

[1]*National Institute of Lasers and Optronics (NILOP), P.O. Nilore 45650, Islamabad, Pakistan*
[2]*Trinity College Dublin, School of Physics, Dublin 2, Ireland*
[3]*Department of Mechanical Engineering, Muhammad Ali Jinnah University, Islamabad, Pakistan*

*Corresponding author. Tel: (+92) 51-9248801, Ext-3053; Fax: (+92) 51-2208051

Received: 28 February 2015, Revised: 03 April 2015 and Accepted: 05 April 2015

ABSTRACT

We report synthesis of the functional ZnO nanostructures (nanowires, nanorods) by a cost effective and efficient method; called composite-hydroxide-mediated (CHM) approach. Effect of the processing temperature on the particle size, morphology, and subsequently morphological dependent optical emissions is investigated. Needle shaped nanowires are obtained at 200 and 220^{o}C, of about (500-1500) nm in length, while at 250^{o}C; nanorods are formed with length in the range of (200-460) nm and width (10-30) nm. Optical study reveals that ZnO nanorods show only ultra-violet (UV) emission while bent nanowires demonstrate both UV and green emissions simultaneously. The week green emission at 2.4 eV indicates no efficient trapping of the photo-generated hole in the nanostructures. Phase purity, crystalline structure, size and chemical nature of the product are probed by XRD, EDX, Raman spectroscopy and FT-IR. The particle size estimated from the spatial correlation phonon confinement model for the E_2 (high) phonon mode. The applied approach is believed to be an efficient, and a direct route for the synthesis of a wide range simple and complex oxide nanostructures for novel electro-optical nanodevices. Copyright © 2015 VBRI Press.

Keywords: SEM; nanorods and nanowires; Raman spectroscopy; optical properties; morphology dependent emissions.

Introduction

Nano functional materials particularly; ZnO, TiO_2, CdO, NiO, and SnO_2 are intrinsically important because of their unique optical, physical and chemical properties that differ significantly from those of their bulk and molecular counterparts **[1]**. Among these oxides, ZnO nanostructures are considered as the most important functional and exceptional research focused materials for their potential applications in multiple key areas such as energy cells, **[2]** sensitive sensors, **[3, 4]** nanoelectronic and optical devices **[5]** and bio-markers **[6]** etc. However, for these applications, morphology and size of the nanostructures is significantly important which are in turn strongly dependent on the temperature and reaction time of the synthesis process. Among the nanostructures, ID nanostructures (nanowires; NWs, nanorods; NRs) have gained considerable research interest due to their anticipated uses as building blocks of nanotechnology **[7]**. Particular attention has been paid to ZnO NWs and NRs because optical devices likely white light emitting diodes (LEDs) can be fabricated by combining n-ZnO nanorods and hollow nanotubes with different p-type materials to form hetero-junctions **[7, 8]**. Along with other promising properties, emission (luminescence) is one of the most promising optical properties of bulk and nanostructured ZnO and has been investigated intensively **[9]**. However, synthesizing nanostructures for optical nanodevices based on ZnO nanowires and nanorods; the stress/strain induced effects on optical luminescence is unavoidable which may cause a red or blue-shift in the near-band-edge (NBE) emission and broadening in the green emission. Stress/strain in the nanostructures is inherent and strongly depends on the morphological structure of the product. From technological point of view, optical emission from the bent structures due to inherently developed stress/strain is a focused research topic of tremendous interest and in particular is under experimental investigation for optical nanodevices applications. Theoretically, optical emission from ZnO nanorods is well known to be the most efficient when the excitation light is polarized along the axial direction of the nanorods **[10, 11]**.

As an abundant and low cost optical material, synthesis of functional ZnO nanoproduct with predictable rational

strategies is a key for the development of gas sensors, chemical sensors, bio sensors, and optical UV and pH sensors **[1-6]**. As the surface to volume ration of NWs/ NRs is very high, therefore surface states are believed to play a significant role on optical absorption, photoluminescence and photo detection properties. A number of methodologies have been employed to prepare ZnO nanomaterials including; vapor phase process, **[12]** jet deposition, **[13]** precipitation method, **[14]** sol-gel, **[15]** template syntheses, **[16]** hydrothermal synthesis **[17]** and solvothermal synthesis, **[13]** etc. However, composite-hydroxide-mediated (CHM) approach is a low temperature, technically sound and environmentally friendly methodology for fabricating a wide range of nanostructures including; complex oxides, hydroxides, simple oxides, sulfides, selenides, tellurides, fluorides and metals **[18-22]**. The developed CHM approach for the synthesis of nanomaterials has the advantages of being a simple and single step process, easy to scale-up and perhaps of low cost. CHM method is based on the slow-reaction which makes possible to control growth kinetics for tuning the size and morphology of the nanostructures. Moreover, versatility and cost-effectiveness of this approach is useful for obtaining crystalline, chemically purified single phase nanomaterials at low temperatures and in overall shorter reaction times compared to other conventionally high temperature synthesis methods. The method is environmentally appealing which arises from its intrinsic scalability, generality and facility as well as its fundamental basis on the use of hydroxides as the reaction medium. Recently, this method has been successfully applied for the synthesis of crystalline CuO nanostructures in the low temperature range **[22]**.

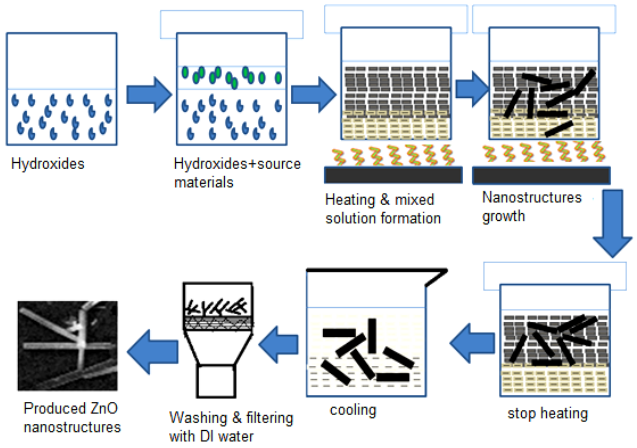

Fig. 1. Illustration of preparation steps of synthesis of the ZnO nanostructures by CHM method**.**

In this research work, we demonstrate composite-hydroxide-mediated (CHM) approach for the synthesis of functionally pure crystalline ZnO nanostructures (nanowires, nanorods). The effect of growth temperature on morphology and subsequently on the optical properties of the nanostructures is investigated. A temperature dependent morphological study is established and luminescent properties of the nanostructures are explored and explained on the basis of stress /strain developed in the bent morphological nanostructure. Finite size effect is employed to estimate crystallite size using spatial correlation model. The observed findings manifest effectiveness of the CHM approach for the synthesis of chemically purified and optically active ZnO nanostructures. The method can be extended to prepare other various nanostructures of technological importance for electro-optical nanodevices.

Experimental

Materials and method

ZnO nanowires/ nanorods were synthesized by CHM method at 200, 220 and 250^{o}C. This method is based on reaction between a metallic salt and hydroxides melts. Zinc oxide nanostructures (NRs and NWs) were prepared from high purity (99.999%, E-Merck) zinc nitrate ($Zn(NO_3)_2.4H_2O$) metallic salt and NaOH/KOH melts. The hydroxides melts were taken in the required ratio NaOH/KOH= 51.5:48.8, mixed with $Zn(NO_3)_2.4H_2O$ salt in a Teflon vessel. The Teflon vessel was placed in the furnace heated at, 200, 220 and 250^{o}C for 12h. Although the melting points of both pure NaOH and KOH are over 300^{o}C, T_m = 323^{o}C for NaOH and T_m = 360^{o}C for KOH, the eutectic point at NaOH/KOH = 51.5: 48.5 is 165^{o}C which is the key for synthesizing simple oxides at much lower temperature. During the reaction process, hydroxides play a crucial role not only as a solvent but also as reactants for lowering the reaction temperature of the process. After reacting for 12h, the vessel was taken out and cooled to room temperature. Deionized water (DI) was added to the solid product. The product was filtered and washed first by deionized water and then hot DI water to remove hydroxide melts on the surface of the product. The preparation steps of ZnO nanomaterials by the CHM method has illustrated in **Fig. 1**.

The synthesized product was received as-produced nanomaterials which are crystalline with clean surfaces, and favorable for further investigations of their intrinsic properties and surface functionalization. Consequently, the reaction mechanism relating to formation of simple ZnO oxides in the hydroxide melts is described as the following (where M denotes Na or K). However, to simplify the chemical reactions here, we only include NaOH in the formula for simplicity;

$$Zn(NO_3)_2.4H_2O + NaOH \rightarrow Zn(OH)_2 + NaNO_3$$

As $Zn(OH)_2$ is chemically not stable and split to form ZnO and water molecules. The ZnO nanostructures so formed are settled down.

$$Zn(OH)_2 \rightarrow ZnO \downarrow + H_2O$$

The growth process of ZnO nanostructures at 220 and 250^{o}C is quite interesting because viscosity is rather low in the hydroxide melts at temperatures higher than 200^{o}C; that greatly increases speed of the nucleus aggregation and recrystallization. Consequently, it results into fast diffusion speed of matter in the melts to keep crystal growing large in the form of nanowires and nanorods.

Characterization of the nanostructures

Scanning electron microscopy system equipped with an Energy Dispersive X-ray Spectroscope (EDS) was used to

observe the morphology and chemical composition of the produced nanostructures.

X-ray diffraction (XRD) analysis of the ZnO nanowires was carried out with Bruker D-8 Discover X-ray diffractometer equipped with a CuKα-radiation (λ=1.54186 Å) source. X-ray source was operated at 40kV and 40mA. The parallel incident X-ray beam was employed with a 0.12° roller slit at the secondary side. The measurements were performed by θ/2θ scans in the 2θ angular range of 25-70° with a step size of 0.02° and at a scan rate of 2°/min.

Room temperature Raman spectroscopy and continuous wave (CW) Photoluminescence (PL) spectroscopy were performed with He-Cd laser as an excitation source emitting wavelengths of 442 and 325 nm used for Raman and photoluminescence measurements respectively. The spectra were collected with a triple grating spectrograph (μ-Ramboss MST-4000A, DONGWOO OPTRON, CO., Ltd.), equipped with a charge coupled device (CCD) and an air cooled detector by using INDOR software. A Fourier transform infrared interferometer (PMQ II, Carl Zeiss) was used to measure the transmittance (T) in the wavelength region of interest.

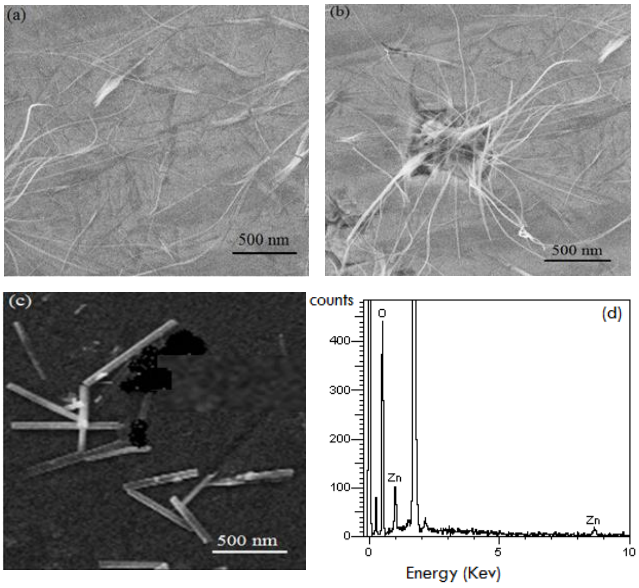

Fig. 2. SEM micrographs of the ZnO nanostructures prepared at (a) 200 °C (b) 220°C (c) 250°C and (d) EDS spectrum showing the presence of Zn and O elements.

Results and discussion

SEM study

The morphology and chemical composition of as synthesized samples prepared at different growth temperatures are shown in **Fig. 2 (a, b, c, d)**. The morphology of prepared ZnO nanomaterials consists of bend, straight nanowires and nanorods. SEM micrograph of the sample prepared at 200°C for 12h **(Fig. 2(a))** is evidently exhibiting nanowires morphology; however, the growth of ZnO nanowires at this temperature is not appropriate. As the process temperature is increased to 220°C, the proper growth and uniform formation of the ZnO nanostructures can be seen in great quantities which are nucleated in the form of nanowires **(Fig. 2(b))**. This in fact consolidates effectiveness and potentiality of the CHM approach for synthesizing ZnO nanowires up to several nanometers long at 220°C. These nanowires are comprised of uniform geometry and dislocation-free volume and up to several nanometers long, i.e. 500–1500 nm. It is worth mentioning that the fascinating needle shaped morphology originating from the common center is an exemplary feature of these NWs. From the observations of the SEM micrograph, ends of these (NWs) exhibit a peculiar morphology, similar to needle-like heads with straight geometry. Some of these nanostructures are not found as straight in their entire length, and kinks with specific angles can be seen. Bending in nanostructure is an important feature particularly of the nanowires and could be quite interesting after growth as such structures can be bent and re-aligned through irradiation. When ZnO nanowires are irradiated with energetic ions, bending and alignment in different directions are achieved and could be use for potential applications. Obviously, the non-bending NWs are more stable because the repulsion induced strains are absent. Captivatingly, the improved photo response performance from straight structured ZnO nanowires and nanorods is believed to be significantly important for optoelectronic and sensor applications.

Interestingly, a significant morphological change is observed in the nucleated nanostructures at reaction temperature of 250°C. At this temperature, nanowires are found in the form of nanorods as shown in **Fig. 2 (c)**. The growth of ZnO nanostructures at 250°C in the form of nanorods is reasonably obvious and quite appealing for fabricating nanodevices. Here it is noteworthy to mention the mechanisms of nanostructures formation and temperature dependent morphological transformation from nanowires into nanorods. In CHM, the growth process of oxide nanostructures is quite interesting because of the temperature dependent viscosity of the melts. At lower temperature, viscosity of the hydroxide melts is rather high that greatly increases speed of the nucleation and consequently aggregation and re-crystallization of nanomaterials. Consequently, it results into fast diffusion speed of the matter in the melts to keep crystal growing smaller or larger in the form of various nanostructures more likely; nanoparticles, nanowires, nanocubes and nanorods etc. Therefore, morphology and perhaps size of the nanomaterial can be tuned by varying the processing temperature. At higher temperature, the crystallites in the nanorods and nanowires achieve an equilibrium shape and nucleate in the form of stable nanostructures. These nanorods can be utilized for the fabrication of LEDs based on crystalline substrates like n-ZnO/p-SiC **[7, 23]**.

In micrograph (Fig. **2 (c))**, different sizes of the ZnO nanorods indicate that the morphology of ZnO from nucleation to growth is predominantly one dimensional. These nanorods are of about 10-30 nm in width and 200-460 nm in length. For evaluation and estimation of purity and surface compositional analysis; energy-dispersive X-ray spectrum (EDS) measurements and analysis has performed. **Fig. 2 (d)** shows EDS survey spectrum of ZnO nanowires which demonstrates no peak of other elements than Zn and oxygen in the sample. This clearly supports synthesis of impurity free ZnO nanostructures by CHM approach.

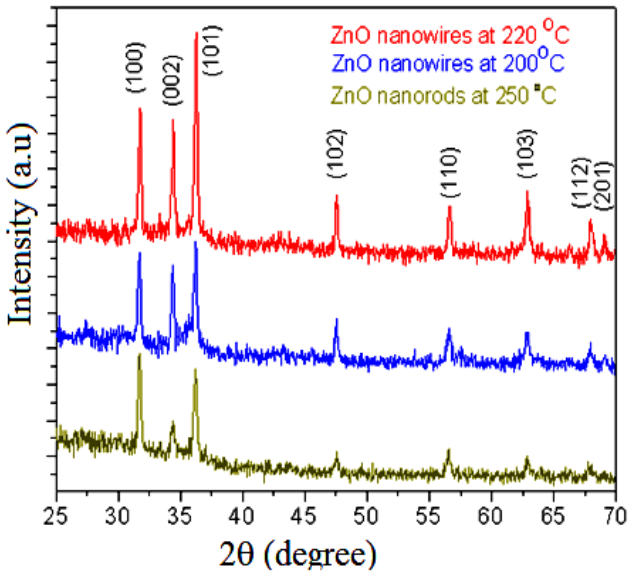

Fig. 3. X-ray diffraction (XRD) pattern of the ZnO nanostructures (nanowires, nanorods) prepared via CHM route (using CuKα radiation λ=1.54186 Å).

XRD analysis

XRD pattern of the ZnO nanostructures (NWs, NRs) has been illustrated in **Fig. 3**. XRD diffractogram shows diffraction peaks of the hexagonal ZnO which are well distinguishable and clearly reveals a significant degree of crystallinity in the product. The prominent intense diffraction peak has indexed as (100) is attributed to *a*-axis whereas (002) to *c*-axis. The lattice constants are determined for all the samples and have values a = 0.3248nm, and c = 0.5370nm (at 200 °C), a = 0.3231nm, and c = 0.5349nm (at 220 °C) and a = 0.3261nm, and c = 0.5382nm (at 250 °C). The modification in the lattice constants can be associated with the morphologies of the nanostructures. The decreased values of a, and c for the bent nanowires may be due to the internally developed compressive stress/strain at the grain boundaries caused by the morphological changes **[24]**. Other possible native imperfections due to morphological changes could also lead to such variation in the lattice constants. It is noteworthy that for the synthesized nanorods; the peak intensity of (002) lattice plane is quite small while (101) plane shows a prominent peak behavior for the product prepared at 250°C. This could be due to size of the scattering domains which may be different from nanowires to nanorods or can be attributed to the preferentially oriented grains in the nanostructures at higher processing temperature. Furthermore, a difference in the diffraction intensities of the diffraction planes in the XRD pattern can be explained in the framework of miller indices (h k l). The peak intensity is determined by the atoms in the diffraction plane and the value of intensity will be different if atoms in the diffracting plane of a unit cell are different or if the atoms in plane are strained due to morphological peculiarities. We are mentioning here that general explanation for the morphology of the ZnO nanostructures is related to the difference in the surface free energies for the main crystallographic planes of hexagonal ZnO: G_{002}=-2.8102 kJ/mol, G_{101}=-2.1067 kJ/mol and G_{100}=-2.0013 kJ/mol, respectively. Due to this anisotropy, preferential growth on the plane of lowest energy occurs, providing the elongated ZnO structures along the c-axis [25]. The other low intensity diffraction peaks seem in ZnO corresponds to the lattice planes indexed as (101), (102), (110), (103), (112), and (201). These diffraction peaks are in close agreement with the joint committee on powder diffraction standards (JCPDS No. 39-1363) and have indicated formation of purely hexagonal-ZnO nanostructures by the CHM method. No diffraction peaks from impurity (traces) like Zn salt, melts or any and other species are not detected which indicates that all the chemicals have been completely decomposed during the reactions and no other crystal products have retained in the product after the chemical process. This also signifies potential of the applied CHM approach for the synthesis of high quality, single phase and pure ZnO nanomaterials. XRD measurements performed on ZnO nanostructures give a strong signature on the aforementioned EDS analysis.

The particle size (D) of the samples is determined using the Scherrer's formula ($D = 0.9\lambda / \beta \cos\theta$) **[24]**. Here D is the particle size, λ the X-ray wavelength and θ the Bragg's angle in radians and β the full width at half maximum of (101) peak in radians. The average size of the crystallite in products is found to be in the range from 44.7-63.4 nm. As the particle size increases, the unit cell volume and microstrain decrease which would modify the lattice constants as discussed before. For further investigation on the nanostructure of the product, we have determined dislocation density using stoke-Wilson equation **[26]** which becomes important in bend structures and is given as;

$$Dislocation\ density\ (\delta) = \frac{15}{aD}\left(\frac{\lambda}{Dcos\theta} - \beta\right)\frac{1}{tan\theta} \quad \text{---------- (1)}$$

Where β is the instrumental corrected broadening (expressed in radians), θ = Bragg's diffraction angle, D = particle size (nm), a = lattice parameter (nm) and λ = wave length (nm). From the calculated dislocation density it is estimated that its value has decreased from 1.3×10^{12} /m^2 to 0.2×10^{12}/m^2. It means more bending in the morphological structure; greater is the dislocation density.

Raman spectroscopy

Room-temperature Raman scattering measurements are performed on all the samples as shown in **Fig. 4**. All the nanostructures exhibit similar Raman spectrum and the observed Raman phonon modes are well consisted with the Raman-scattering spectra of ZnO **[27, 28]**, however, the E_2 (low)+B_1 (high) mode is observed only for the nanorods. Raman frequencies of both polar and nonpolar optical phonons are found shifted in the spectra obtained from ZnO nanostructures compared to their positions in the reported spectra of bulk ZnO **[27]**.

The observed frequency shift in the samples is due to quantum confinement effect in the nanostructures or may be due to the internal developed stress/strain. Highly intense sharp peak of the principle phonon mode reveals the formation of high-quality crystalline wurtzite structured ZnO NWs and nanorods. The E_2 (high) mode is located at 433.5 cm^{-1} and corresponds to a non-polar optical phonon E_2 (high) mode of wurtzite ZnO and is the characteristic feature of the hexagonal-phase of ZnO **[29]**.

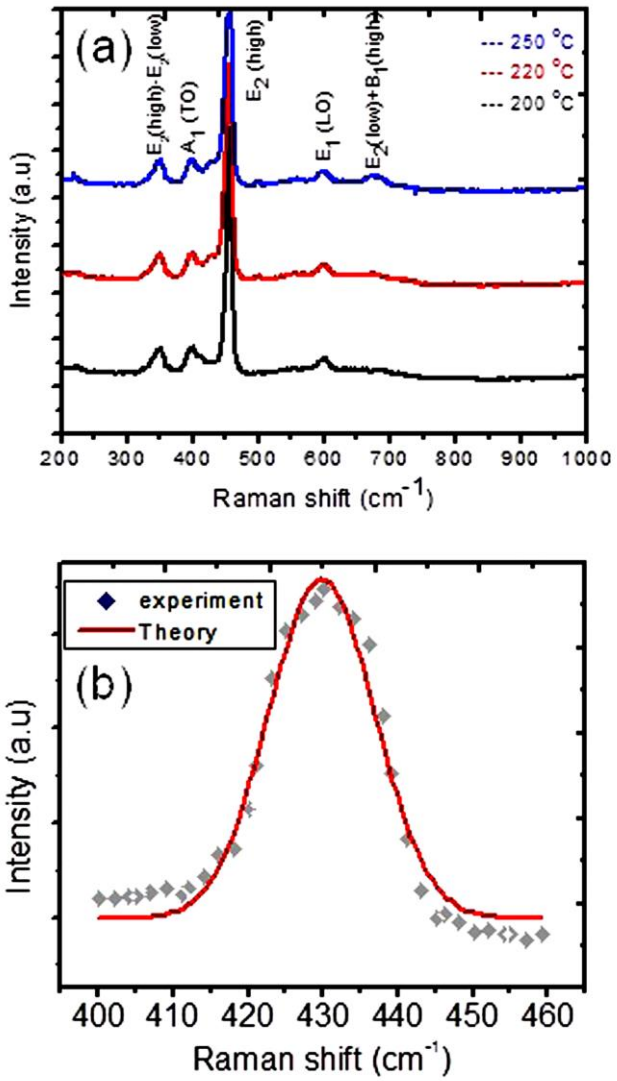

Fig. 4. Room temperature Raman spectrum of the ZnO nanowires prepared at process temperatures (a) 200°C, 220°C and 250°C, and (b) theoretical fitting to the principal phonon E_2 (high) mode using spatial correlation mode.

Its position is shifted by 3.5 cm^{-1} compared to bulk ZnO which can be associated with the quantum confinement effect and other stress/strain aftermath and most probably is observed for the bent nanowires. The phonon frequency band at 378 cm^{-1} agrees with the phonon frequency of A_1(TO) mode of wurtzite ZnO. The Raman peak at 330 cm^{-1} is assigned to the second-order Raman scattering arising from the zone-boundary phonons of hexagonal ZnO involving acoustic phonons and is well consisted with previously reported data on wurtzite ZnO nanocrystals **[29, 30]**. The peak at 578 cm^{-1} is attributed to E_1(LO) mode of h-ZnO, and is associated with oxygen deficiency (oxygen defects). In order to account for a good crystalline quality of the produced nanostructures, there are several indicatives like the signals attributed to the two-phonon density of states (DOS) expected in the spectral range from 600 to 1000 cm^{-1} **[31]** is no longer observed in the sample; the line-width of about 5.4 cm^{-1} corresponding to E_2(high) mode which is comparable to the values reported for high quality ZnO bulk crystals **[32]**; and position of the E_2 (high) peak corresponds to phonon of bulk ZnO crystal indicating a strain-free state of the nanowires.

The average size of NWs and NRs can be determined using a phenomenological phonon confinement model **[33]**. This model is based on the uncertainty of the phonon momentum, because of the reduced size of the structures. In reduced size structures phonons with $q \neq 0$ are allowed to contribute to the Raman spectrum. The phenomenological models use different localization functions. In order to determine size of the particle of NWs and NRs, the

Raman bands were fitted according to a modified correlation length model given bellow. Assuming a Gaussian localization factor the Raman intensity can be expressed as:

$$I(\omega) \propto \int_0^1 \frac{4\pi q^2 \exp\left(-q^2L^2/4\right)}{(\omega - \omega(q))^2 + (\Gamma_o/2)^2} dq \quad \text{---------- (2)}$$

Where q is the wave vector expressed in units of $2\pi/a$, a' is the lattice constant, and Γ_o is the FWHM of the intrinsic Raman line shape of the end-point materials, L is the diameter of the confinement volume expressed in units of the lattice parameter. The expression exp $(-q^2L^2/4)$ represents a Gaussian spatial correlation function and ω (q) is the function of Raman phonon dispersion.

Since in defects free pure ZnO, the E_2 (high) phonon mode has Lorentzian line shape ($\Gamma_a = \Gamma_b$) with a natural line-width $\Gamma_o = (\Gamma_a + \Gamma_b)$ of 2.5 cm^{-1}. While for the dispersion ω (q) of the E_2 (high) phonon mode, we take analytical model relationship based on a one-dimensional linear-chain model for the prepared NWs with small diameter;

$$\omega(q) = A + B\cos(\pi q) \quad \text{---------- (3)}$$

Where for ZnO; A = 424.5 cm^{-1}, and B = 12.5 cm^{-1} respectively. By fitting the E_2 (high) line shape to Eq. 1 and Eq. 2 'L' values for morphological structures are found to be as 7.6482 (at 200°C), 7.6378 (at 220°C) and 7.6281 (at 250°C). The experimental and theoretical fitted E_2 (high) phonon mode is also shown in the same **Fig. 4** for ZnO nanowires. These values are calculated by fitting the Raman spectra of the samples corresponding to different growth temperatures on the Eq. (2) and Eq. (3). The Raman line of ZnO can be described by the dependence of the half-width on the inverse of grain size, which follows a linear behavior; Γ (cm^{-1}) = 10 + 124.7/d_g (nm) and is used to determine materials microstructure and particle size based on the following empirical formulas:

$$\omega(L) = \omega_0 + A\left(a/L\right)^{\gamma} \quad \text{---------- (4)}$$

$$\Gamma(L) = \Gamma_0 + B\left(a/L\right)^{\gamma'} \quad \text{---------- (5)}$$

Where ω(L) and Γ (L) are individual Raman frequency and bandwidth in a nanocrystal with size L, parameters A, B, γ and γ′ are relative to phonon confinement. By fitting

the experimental data A and γ are equal to 424 cm^{-1} and 1.32; B and γ′ are equal to 12.5 cm^{-1} and 1.29. The particles sizes so obtained are in the range from 39.7-60.2 nm. The *L* values obtained can be correlated with the grain size and energy band-gap of the material to see how these structural and optical properties are affected by the "*L"* values. As the correlation-length decreases, band-gap energy of ZnO decreases while grain size "*D"* shows a counter behavior and increases as "*L"* get decreases and is well fitted in the framework of the study.

FT-IR study

Fig. 5. shows FT-IR spectrum of ZnO NWs prepared by CHM approach at 220°C. The spectrum shows three absorption bands located at 498, 529 and 632cm^{-1} respectively. The observed absorption frequency bands at 498 and 529cm^{-1} correspond to the bending mode of Zn-O **[34]**. Apart from these bending bands, the absorption band peaked at 632cm^{-1} is attributed to Zn-O stretching vibration band of nano crystalline ZnO NWs and well consisted with the established theoretical IR study of ZnO **[34, 35].** The presence of absorption peaks associate with ZnO bonding in the spectrum suggests formation of pure ZnO NWs and very well accordance with EDS, Raman and XRD analysis.

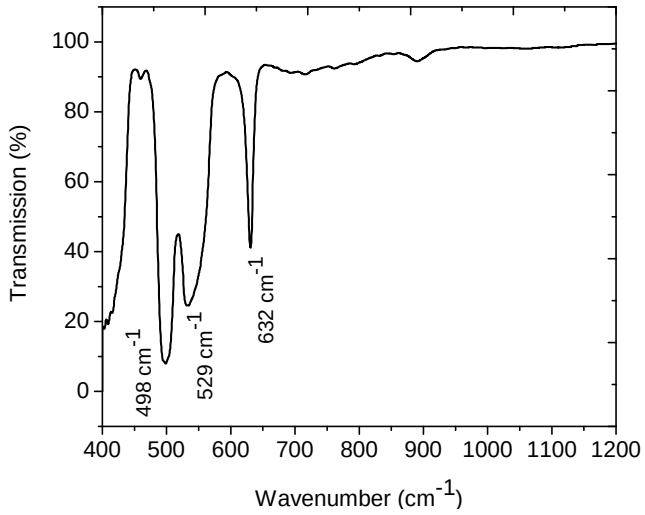

Fig. 5. FT-IR spectrum of the ZnO nanowires prepared by CHM method at 220°C processing temperature.

Photoluminescence spectroscopy

Fig. 6. demonstrates photoluminesecent property of ZnO nanostructures prepared by CHM approach. PL study has revealed high optical quality of the nanostructures. Continuous-wave (CW) PL spectra of the ZnO nanowires at 200 and 220°C show similar behavior and both exhibits near band-edge (NBE) ultra-violet (UV) emission. However, nanowires with bent morphology show both UV and green emissions simultaneously. However, the nanowires with straight morphology throughout their entire length demonstrate only UV emission similar to nanorods. Spectrum of the nanorods clearly shows only single UV emission similar to nanowires with straight morphology. For the nanowires with bent morphology, the UV emission is peaked at 385 nm while green emission at around 518 nm. The UV emission peaked at 385 nm is ascribed to the near-band-edge emission of the wide band gap ZnO due to the extinguishing of exciton, probably caused by the quantum confinement effect **[36]**, while the blue–green emission has attributed to the presence of defects more likely oxygen vacancies. Furthermore, as the centre energy of green emission peak (2.4eV) is smaller than the band gap energy of ZnO (at room temperature 3.4eV), the green emission must be related to a local level in the band gap **[37]**. Interestingly, green emission is observed only for the ZnO nanowires (**Fig. 6** inset, black curve), while for ZnO nanorods, only UV emission is observed.

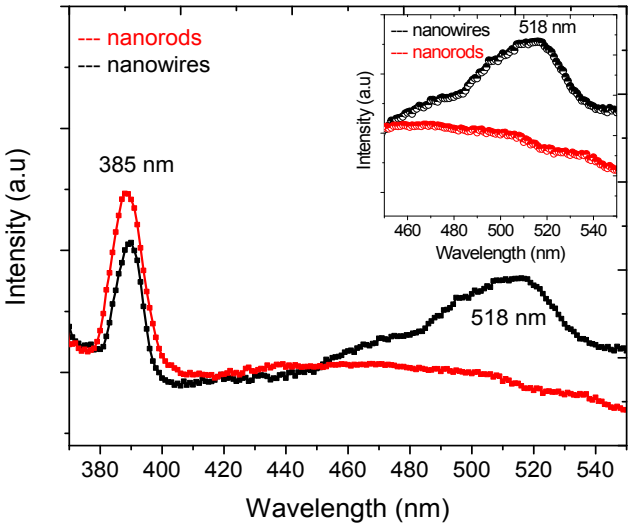

Fig. 6. Room temperature PL spectrum of the ZnO nanostructures (nanowires and nanorods), (the inset shows the green emission observed for the bent nanowires only).

These results are quite appealing regarding bent morphology of the nanowires for optoelectronic applications. It has been reported that nanostructures (NWs, NRs) without bending in their morphology are promising to demonstrate an enhanced near band edge ultraviolet emission whereas deep green emission is totally suppressed **[38]**. The peak energy of the bent NWs is slightly red-shifted compared to as-grown non-bent NWs and nanorods (peaked at 383 nm). Our results indicate that red-shift in the UV emission peak is related to uniaxial compressive stress/strain and enhanced exciton–phonon coupling strength in the bent ZnO NWs. Photoluminescence (PL) emission in bent ZnO NWs is mainly caused by the strain-induced changes in the energy band structure together with the other micro-structural effects, which modifies the spatial local distribution of photoexcited carriers. This effect is also further reflected in the tail of the PL spectrum on longer wavelength side. The corresponding red-shift can be estimated and correlated with particle size using the well-known Brus equation based on effective mass model **[39, 40**];

$$\Delta E = \frac{h^2}{8\mu R^2} + \frac{1.8e^2}{4\pi R \varepsilon_0 \varepsilon_\infty} \text{ ---------- (6)}$$

Where $\mu = (1/m_e^* + 1/m_h^*)$, *and* m_e^*, m_H^* are the effective masses of a conduction band electron and valence

band hole in ZnO ($m_e^* = 0.18$ and $m_H^* = 0.25$), for ZnO), e_∞ the high-frequency dielectric constant and R the diameter of the particle. This red-shift is the predominant behavior of the developed strain in the bent structure of the product. The peak wavelength in the PL spectrum is used to determine particle size using the above equation based on effective mass approximation. The simplified form of the above Eq. derived using the effective mass model describe the particle size (r, radius in nm) as a function of peak emission wavelength (λ_p) can be written as;

$$r(nm) = \frac{-0.3049 + \sqrt{-26.23012 + \frac{10240.72}{\lambda_p(nm)}}}{-6.3829 + \frac{2483.2}{\lambda_p(nm)}} \quad (7)$$

For peak wavelength (λ_p) of nanosized ZnO, the particle size is determined to make a comparison of the sizes at various process temperatures. The particle sizes ($D=2r$) determined are about 54.6-61.3 nm and are closely consisted with those estimated by Raman, and XRD.

The PL results are well supported by the Raman analysis showing a blue shift in the principle E_2 (high) Raman phonon mode. In the PL spectra, low energy tail on the longer wavelength side in the ZnO nanostructures is quite evidently seemed for all the samples. This tail can be obliged to LO phonon replica due to strong exciton-phonon coupling in ZnO. The tail effect at the longer wavelength side and asymmetric line-width in the PL spectrum clearly indicates that the different optical transition processes are responsible for the near band edge emissions. Furthermore, the extended tail is usually caused by the band structural deformation resulting from the lattice deformation in nanostructures due to strain induced effects. The fractional intensity for bound exciton (BX) transitions is shown to be correlated with the size in all these ZnO nanostructures while the long tail may be attributed to the inhomogeneous density distribution of the defects as binding sites in the ZnO nanostructures. The long tail of the defect related emission can also be related to the non-uniform defects density in at the grain boundaries of the nanostructures. Furthermore, surface band bending, instead of the oxygen vacancy concentration, are shown to be the mechanism that determines the observed changes in photoluminescence particularly the broad band of green emission with extended long energy tail.

From the in-set in **Fig. 6**, it is also clear that intensity of the green visible emission band is much lower than that of the exciton emission band. As both emission processes compete with each other and this means that the visible emission process must involve a step in which the photo-generated hole is not trapped efficiently in the particle. To have strong visible emission, the rate of this hole' trapping must be much faster than the radiative recombination rate of the exciton emission. Because of the large surface-to-volume ratio of our ZnO nanowires, efficient and fast trapping of photo-generated holes at surface sites can be expected. A probable candidate for the trapping of holes are O_2~ ions at the surface of the nanostructures **[41, 42]**. Trapping of a photo-generated hole at the surface is also in agreement with size-dependence of the emission intensities. The transition rate for a surface trapping process decreases as the particle size increases since the surface to-bulk ratio decreases. The transition rate of the exciton recombination will not be influenced strongly by the particle size.

Conclusion

A low temperature, single step, technically feasible and environmentally friendly synthesis approach the so called composite-hydroxide mediated (CHM) was realized and demonstrated for the synthesis of ZnO nanostructures (nanowires and nanorods). The nanostructures were needle shaped aggregated nanowires of about 500-1500 in length and nanorods of (10-30) nm in width and (200-460) nm in length. By increasing the process temperature, morphology of the nanostructures transformed from nanowires (at 220^{o}C) into nanorods (at 250^{o}C). XRD and Raman analysis indicated the formation of highly pure hexagonal-ZnO nanostructures with no impurity traces. FT-IR study demonstrated chemical nature and bending, stretching bonding of ZnO. Two PL peaks were observed at 385nm and 518nm corresponding to excitonic UV and green luminescence of ZnO for the nanowires with bent morphology. For the bent morphology of the nanowires, stress and strain developed within the structure were accounted for the green emission. Nanorods and nanowires with straight morphology showed only UV emission which is useful for the UV nanodevices. A weak green emission for the bent nanowires indicated that photo-generated holes are not trapped efficiently in the particle and represented lesser number O_2~ ions at the surface. The advantages of the method; rapid synthesis, in a normal atmosphere, with 100% productive ratio and at low cost, give a potential avenue for further practical scale-up of the production process and applications of novel devices based on nanorods and nanowires.

Acknowledgements

We gratefully acknowledge the research facilities of PINSTECH and NILOP research centres for this research work. We are also thankful to Mr. Khurram Shahzad, Physics Division for his help and cooperation.

Reference

1. Guo, Y.; Hu, J.; Wan, L. *Adv. Mater.* **2008**, *20*, 2878. **DOI**: 10.1002/adma.200800627
2. Shao, Z.; Haile, S.; *Nature* **2004**, *431*, 170. **DOI**: 10.1038/nature02863
3. Zhou, J.; Fei, P.; Gu, Y.; Mai, W.; Gao, Y.; Yang, R..; Bao, G.; Wang, Z.; *Nano. Lett.* **2008**, *8*, 3973. **DOI:** 10.1021/nl802367t
4. Shang, L.; Dong, S. J.; *Mater. Chem.* **2008**, *18*, 4636. **DOI:** 10.1039/B810409C
5. Voss, T.; Svacha, G.T.; Mazur, E.; Muller, S.; Ronning, C.; Konjhodzic, D.; Marlowet, F.; *Nano Lett.* **2007**, *7*, 3675. **DOI:** 10.1021/nl071958w
6. Chai, G.; Lupan, O.; Chow, L.; Heinrich, H.; *Sens. Actuat. A* **2009**, *150*, 184. **DOI:** 10.1016/j.sna.2008.12.020
7. İkizler, B.; Peker, S.; *Adv. Mat. Lett.* **2014**, *5*, 325. **DOI:** 10.5185/amlett.2014.amwc.1020
8. Vinod, K.; Vijay, K.; Som, S.; Duvenhage, M.M.; Ntwaeaborwa, O.N.; Swart. H.C.; *Appl Chem. Eng. J.* **2014**, *255*, 541. **DOI:** 10.1016/j.cej.2014.06.027
9. Willander, M.; Nur, O.; Sadaf, J.R.; Qadir, M.I.; Zaman, S.; Zainelabdin, A.; Bano, N.; Hussain, I.; *Materials* **2010**, *3*, 2643.

DOI: 10.3390/ma3042643
10. Ruda, H.E.; A. Shik, A.; *Phys. Rev. B* **2005**, *72*, 115308. **DOI:** 10.1103/PhysRevB.72.115308
11. Chen, H.Y.; Yang, Y.C.; Lin, H.W.; Chang, S.C.; Gwo, S.; *Opt. Express* **2008**, *16*, 13465. **DOI:** 10.1364/OE.16.013465
12. Pan, Z.; Dai, Z.; Wang, Z.; *Science* **2001**, *291*, 1947. **DOI:** 10.1126/science.1058120
13. Sanjay, S.S.; Yadav, R.S.; Pandey, A.C.; *Adv. Mater. Lett.* **2013**, *4*, 378. **DOI:** 10.5185/amlett.2012.9427
14. Yadav, T.P.; Mukhopadhyay, N.K; Tiwari, R.S; Srivastava, O.N.; *J. Nanosci. Nanotechnol.* **2007**, *7*, 575. **DOI:** 10.1166/jnn.2007.128
15. Hartridge, A.; Bhattacharya, A.K.; *J. Phys. Chem. Solids* **2002**, *63*, 441. **DOI**: 10.1016/S0022-3697(01)00158-5
16. Huczko, A.; *Appl. Phys. A* **2000**, *70*, 365. **DOI:** 10.1007/s003390051050
17. Baruwati, B.; Kumar, D.; Manorama, S. *J.; Sens. Actuators. B: chem.* **2006**, *119*, 676. **DOI:**10.1016/j.snb.2006.01.028
18. Liu, H.; Hu, C.G.; Wang, Z.L.; *Nano Lett.* **2006**, *6*, 1535. **DOI**: 10.1021/nl061253e
19. Kuriakose, S.; Satpati, B.; Mohapatra, S.; *Adv. Mater. Lett.* **2015**, *6*, 217. **DOI:** 10.5185/amlett.2015.5693
20. Wang, N.; Hu, C.G.; Xia, C.H.; Feng, B.; Zhang, Z.W.; Xi, Y.; Xiong, Y.F.; *Appl. Phys. Lett.* **2007**, *90*, 163111. **DOI:** 10.1063/1.272269
21. Hu, C.C.; Zhang, Z.W.; Liu, H.; Gao, P.X.; Wang, Z.L.; *Nanotechnology* **2006**, *17*, 5983. **DOI:** 10.1088/0957-4484/17/24/013
22. Liu, M.; Jin, H.; Liu, M.; Dong,J.; Hou, P.; Ji, Z.; Hou, S.; *Cryst. Res. Technol.* **2014**, *49*, 820. **DOI:** 10.1002/crat.201400190
23. Willander, M.; Nur, O.; Bano, N.; Sultana, K.; *New J. Phys.* **2009,** *11*, 125020. **DOI:** 10.1088/1367-2630/11/12/125020
24. Usseinov, A.B.; Kotomin, E.A.; Zhukovskii A.T.; Puans, J.; *Thin Solid Films* **2014**, *553*, 38. **DOI:** 10.1016/j.tsf.2013.11.021
25. Fujimura, N.; Nishihara, T.; Goto, S.; Xu, J.; Ito, T.; *J. Cryst. Growth* **1993**, *130*, 269-279. **DOI:** 10.1016/0022-0248(93)90861-P
26. Khan, T.M.; *J. Mater. Chem. Phys.* **2015**, *153*, 248. **DOI:** 10.1016/j.matchemphys.2015.01.011
27. Zhou, K.; Wang, X.; Sun, X.; Peng, Q.; Li, Y. J.; *Catalysis* **2005**, *229*, 206. **DOI:** 10.1016/j.jcat.2004.11.004
28. Ashkenov, N.; Mbenkum, B.; Bundesmann, C.; Riede, V.; Lorenz, M.; Spemann, D.; Kaidashev, E.M.; Kasic, A.; Schubert, M.; Grundmann, M.; Wagner, G.; Neumann,H.; Darakchieva, V.; Arwin, H.; Monemar, B.; *J. Appl. Phys.* **2003**, *93*, 126. **DOI:** 10.1063/1.1526935
29. Serrano, J.; Manjo´n, F. J.; Romero, A. H.; Widulle, F.; Lauck, R.; Cardona, M.; *Phys. Rev. Lett.* **2003** *90*, 055510. **DOI:** 10.1103/PhysRevLett.90.055510
30. Wang, Y.; Leu, I.; Hon, M.; *J. Mater. Chem.* **2002**, *12*, 2439. **DOI:** 10.1039/B111189M
31. Rajalakshmi, M.; Arora, A.K.; Bendre, B.S.; Mahamuni, S.; *J. Appl. Phys.* **2000**, *87*, 2445. **DOI:** 10.1063/1.372199
32. Serrano, J.; Romero, A. H.; Manjon, F. J.; Lauck, R.; Cardona, M.; Rubio, A.; *Phys. Rev. B* **2004**, *69*, 094306. **DOI:** 10.1103/PhysRevB.69.094306
33. Manjon, F.J.; Mollar, M.; Fenollosa, M.; Marı, B.; Lauck, R.; Cardona, M.; *Solid State Commun.* **2003** *128*, 35. **DOI:** 10.1016/S0038-1098(03)00616-1
34. Lupan, O.; Emelchenko, G.; Ursaki, V.; Chai, G.; Redkinf, A.; Gruzintsev, A.; Tiginyanu, I.; Chow, L.; Ono, L.; Cuenya, B.; Heinrich, H.; Yakimov, E.; *Mater. Res. Bullet.* **2010**, *45*, 1026. **DOI:** 10.1016/j.materresbull.2010.03.027
35. French, S.A.; Sokol, A.A.; Bromley, S.T.; Catlow, C.R.A.; Rogers. S.C.; Sherwood, P.; *J. Chem. Phys.* **2003**, *118*, 317. **DOI:** 10.1063/1.1523897
36. Kumar, V.; Vijay, K.; Som, S.; Neethling, J.H.; Lee, M.; Ntwaeaborwa,O.M.; Swart, H.C.; *Nanotechnology* **2014**, *25*, 135701. **DOI:** 10.1088/0957-4484/25/13/135701
37. Lin, B.; Fu, Z.; Jia, Y.; *Appl. Phys. Lett.* **2001**, *79*, 943. **DOI:** 10.1063/1.1394173
38. Chen, R.; Ye, Q.; He, T.; Wu, T.; Sun, H.; *Appl. Phys. Lett.* **2011**, *98*, 241916. **DOI:** 10.1063/1.3601479
39. Khan, T.M.; Iqbal, A.; Zakria, M.; *Vacuum* **2014**, *105*, 1. **DOI:** 10.1016/j.vacuum.2014.01.027
40. G. Schoenmakers, G.; Vanmaekelbergh, D.; Kelly, J.J.; *J. Phys. Chem.* **1996**, *100*, 3215. **DOI:** 10.1021/jp952392f
41. Piscanec, S.; Cantoro, M.; Ferrari, A.C.; Zapien, J.A.; Lifshitz, Y.; Lee, S.T.; Hofman, S.; Robertson, S.; *Phys. Rev. B* **2003**, *68*, 241312(R). **DOI:** 10.1103/PhysRevB.68.241312
42. Vinod, K.; Vijay, K.; Som, S.; Duvenhage, M.M.; Ntwaeaborwa, O.N.; Swart. H.C.; *Appl. Surf. Sci.* **2014**, *308*, 419. **DOI:** 10.1016/j.apsusc.2014.04.192